CORROSION SCIENCE AND TECHNOLOGY, Vol.20, No.5(2021), pp.231~241 pISSN 1598-6462 / eISSN 2288-6524
[Research Paper] DOI: https://doi.org/10.14773/cst.2021.20.5.231

Electrochemical Frequency Modulation: Solution Resistance and Double Layer Capacitance Considerations

Shashi Lalvani[1,†], Sifat Ullah[2], and Lei Kerr[1]

[1]*Chemical, Paper and Biomedical Engineering, Miami University, Oxford, Ohio 45056*
[2]*Mechanical and Manufacturing Engineering, Miami University, Oxford, Ohio 45056*
(Received April 07, 2021; Revised June 22, 2021; Accepted September 02, 2021)

The objective of this study was to evaluate total current under steady-state conditions for a material undergoing corrosion using the electrochemical frequency modulation (EFM) technique, taking into account the presence of solution resistance and double layer capacitance. The analysis involving linearization of the Tafel curve allowed for the estimation of corrosion parameters. Results showed that the output signal was dependent on fundamental frequencies and their multiples. In addition, the output signal almost manifested itself at frequencies that were sums of fundamental frequencies of the applied sinusoidal signal. The harmonics calculated showed a significant shift from the principal frequency of input signals. The investigation involved the influence of corrosion current and anode-to-cathode Tafel slope ratio on faradaic and non-faradaic currents (including the average and RMS). The model presented showed both qualitative and quantitative improvements over the previously developed EFM technique that ignored the influence of solution resistance and the double layer capacitance while assuming the applied DC potential corresponded to the corrosion potential of the corroding material.

Keywords: *Modulation, Corrosion, EFM, Frequency*

Nomenclature

β_a : anodic Tafel slope, V
β_c : cathodic Tafel slope, V
c_d : double layer capacitance, F/cm^2
f : frequency(= $\frac{\omega}{2\pi}$), cycles per second (Hz)
i_{corr} : corrosion current (in absence of alternating field), A
i_f : faradaic current, A
i_{nf} : non-faradaic current, A
i_t : total current, A
E : potential across R_f or C_{dl}, V
E_{Corr} : corrosion potential (in absence of alternating field), V
E_{DC} : applied DC potential, V
E_P : peak potential, V
E_t : total potential, V
R_s : solution resistance, ohms
Z_P : charge transfer impedance, ohms
ω : frequency (= $2\pi f$), radians/s
ϕ : shift in phase anlge

1. Introduction

About two decades ago Bosch *et al.* [1,2] introduced a new technique called Electrochemical Frequency Modulation (EFM) to analyze the corrosion behavior of metals and alloys. This method was a development of earlier work by Rao and Mishra [3], Bertoia [4], and Meszaros [5].

The basic principle involves the perturbation of a corroding system by the application of two sinusoidal potential inputs of fairly small equal magnitudes at different frequencies. The analysis based upon the linearization of the Tafel equation shows the resultant current consists of harmonics of the principal frequencies of the applied signals as well as the other higher-order harmonics that consist of the multiples and sums (and differences) of the two principal frequency modulations [1]. By introducing the harmonic and intermodulation parts in expressing them in terms of "causality factors", the authors [1,2] have been successful in estimating the corrosion parameters. Since then, a number of papers have reported corrosion measurements using the EFM

[†]Corresponding author: lalvansb@miamioh.edu

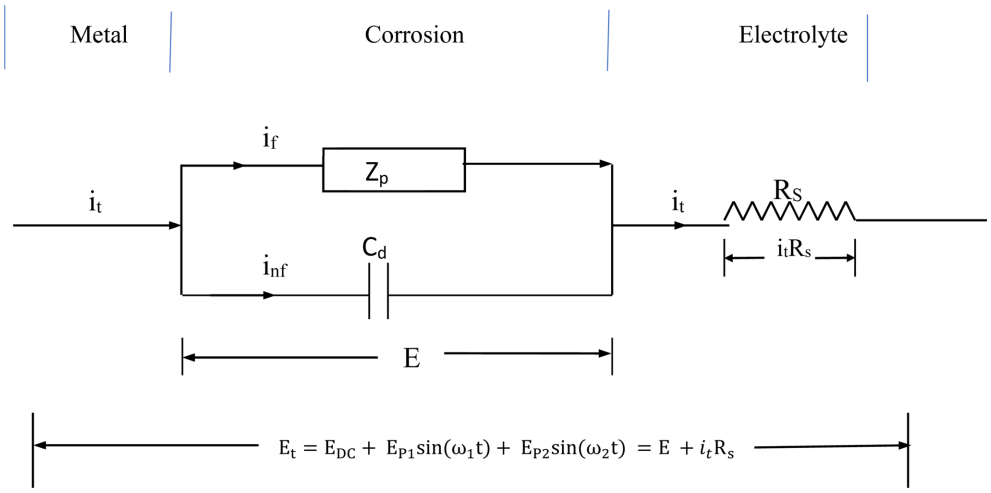

Fig. 1. A schematic of different elements that describe corrosion of the material

technique. A recent review by Obot and Oneyeachu [6] provides a comparison of EFM with other contemporary electrochemical techniques for corrosion measurement. Rauf and Mahdi [7] have used EFM to study pitting corrosion. In another study, Rauf *et al*. [8] have applied the technique to analyze stress corrosion cracking. Singh *et al.* [9] have applied the EFM technique to evaluate the corrosion rate of a corroding material in the presence of inhibitors of acridinedione. Danee and Nipaska [10] have recently studied modification of the corrosion behavior of steel in the presence of a corrosion inhibitor using the EFM technique.

Thus, a growing interest in the application of EFM to study corrosion is reported in the literature. The original work by Bosch *et al*. [1] and the subsequent work since then does not take into account either the influence of the double-layer capacitance or the solution resistance on deriving the expressions for the current, and as a result the peak currents associated with the principal and intermodulation excitation frequencies are found to be independent of the frequency. Of course, it is an aberration since the double-layer capacitance is known to increase with the frequency. The experiemental data which employs EFM methods has indeed shown that the causality factors (which are functions of the peak currents) are indeed functions of time and in many instances exhibit periodic behavior [7,12,13] In addition, some of the data appear to show a slight phase shift in the harmonics from the theoretical calculated values [11]. The model also does not explain the potential peaks as a function of frequency as observed in the experimental data [12]. In a recent paper, Lalvani *et al*. [14] have corrected algebraic errors involved in the mathematical treatment of the problem by Bosch *et al*. [1,2].

As shown by the schematic of a typical corroding system in Fig. 1 [15], the presence of a double layer results in a potential (E) that drives the rate of corrosion (i.e. faradaic current), which is lower than the total applied potential. The following model takes into account the presence of a double layer present on the surface of the electrode and the solution resistance. The impedance corresponding to the charge transfer is represented by Z_p. The first step in the solution to the model involves the linearization of the Tafel equation used in the voltage balance across the circuit shown in Fig. 1. It allows for the estimation of the potential E, to which the corroding specimen is subjected to. This in turn allows for the estimation of the faradaic current from the Tafel equation (expanded to the fourth term in the series). In an earlier analysis presented by Bosch *et al*. [1], the two impressed peak potentials in EFM are assumed to equal in magnitude. In addition, the model assumes the DC potential corresponds to the corrosion potential of the specimen whose corrosion behavior is being studied. By considering the two signals to have unequal peaks not only presents a more general treatment of the problem, but it allows the experimentalist to have greater control on the process parameters to study corrosion.

2. Model Development

The total applied potential (E_t) across the working electrode is the sum of a DC potential (E_{DC}) and two sinusoidal potential functions (E_{P1} sin $\omega_1 t$ and E_{P2} sin $\omega_2 t$) as shown by the following equation:

$$E_t = E_{DC} + E_{P1} \sin(\omega_1 t) + E_{P2} \sin(\omega_2 t) \quad (1)$$

In the above equation $\omega = 2\pi f$ with the frequency, f is in hertz (cycles/second). The total potential can be written as the sum of the potential drop across the resistor (and the potential generated across the double layer capacitance, E) as shown in Fig. 1.

$$E_t = E + i_t R_s \quad (2)$$

Where i_t and R_s represent the total current and the solution resistance respectively. The total current in turn is the sum of the faradaic current (i_f) and the non-faradaic (i_{nf}) currents:

$$i_t = i_f + i_{nf} \quad (3)$$

The following Tafel equation describes the faradic current

$$i_f = i_{corr}\left[e^{\frac{E-E_{corr}}{\beta_a}} - e^{\frac{-(E-E_{corr})}{\beta_c}}\right] \quad (4)$$

where i_{corr}, E_{corr}, β_a, β_c are respectively, the corrosion current, corrosion potential, the anodic Tafel slope, and the cathodic Tafel slope. The non-faradaic current is the current flow across the double layer capacitance (i_{cd}) and is given by the following expression:

$$i_{nf} = i_{cd} = C_d \frac{dE}{dt} \quad (5)$$

In the above equation, C_d stands for the double-layer capacitance. Substitution of equations 4 and 5 and in equation (3) allows for evaluation of the total current, which along with equations (1) and (2) leads to the following nonlinear first-order differential equation:

$$\frac{dE}{dt} + \frac{i_{corr}}{c_d}\left[e^{\frac{E-E_{corr}}{\beta_a}} - e^{\frac{-(E-E_{corr})}{\beta_c}}\right] + \frac{E}{R_s c_d} = \frac{E}{R_s c_d} + \frac{1}{R_s c_d}\left[E_{P1}\sin(\omega_1 t) + E_{P2}\sin(\omega_2 t)\right] \quad (6)$$

The first two terms of the expansion of the exponents in the Tafel equation allow us to linearize the differential equation, and thus we obtain:

$$\frac{dE}{dt} + \alpha E = \lambda + \gamma_1 \sin(\omega_1 t) + \gamma_2 \sin(\omega_2 t) \quad (7)$$

The solution to the linearized differential equation is given by:

$$E = a_o + a_1 \sin(\omega_1 t - \phi_1) + a_2 \sin(\omega_2 t - \phi_2) + c_o e^{-\alpha t}$$

where C_o is the constant of integration while the other coefficients are listed in the Appendix. The steady-state solution is:

$$E = a_o + a_1 \sin(\omega_1 t - \phi_1) + a_2 \sin(\omega_2 t - \phi_2) \quad (8)$$

Thus, it is seen that the potential across the faraday impedance (Z_p) is not only unequal to the applied total potential at the electrode, but it exhibits a phase shift in the sinusoidal component (ϕ). The phase shift is a function of the signal frequency and the Tafel slopes. The various constants appearing in the above and also in other expressions found in the paper are defined in Appendix. Expansion of the exponents in equation (4) and neglecting the fourth-order and higher terms gives us the faraday current in terms of the potential, E.

$$i_f \cong i_{corr}[\alpha_1(E-E_{corr}) + \beta_1(E-E_{corr})^2 + \gamma_1(E-E_{corr})^3] \quad (9)$$

Substituting for E from equation 8 into equation 9 allows for the development of faradaic current in terms of the input sinusoidal functions as described below:

$$\begin{aligned} i_f = {} & A + B\sin(x) + C\sin(y) + D\cos(2x) + E1\cos(2y) \\ & + F\sin(3x) + G\sin(3y) + H[\cos(x\text{-}y) - \cos(x+y)] \\ & + I\cos(2x)\sin(y) + J\sin(x)\cos(2y) \end{aligned} \quad (10\text{-a})$$

Where

$$x = (\omega_1 t - \phi_1) \quad (10\text{-b})$$
$$y = (\omega_2 t - \phi_2) \quad (10\text{-c})$$

Where x and y correspond to the primary phase shift. Unlike in the previous work [1-5], it is observed that in addition to the principal frequencies of the intermodulation, the faradaic current is also proportional to the phase shift in the signal frequencies corresponding to angles ϕ_1 and ϕ_2.

The last two terms in equation (10-a) can be expressed in terms of sine functions involving the sums of 2x, 2y and x and y. Thus, it is possible to express the equation as follows:

$$\begin{aligned} i_f = {} & A + B\sin(x) + C\sin(y) + D\cos(2x) + E1\cos(2y) \\ & + F\sin(3x) + G\sin(3y) + H[\cos(x-y) - \cos(x+y)] \\ & + \frac{1}{2}[\sin(2x+y) - \sin(2x-y)] + \frac{J}{2}[\sin(2y+x) \\ & - \sin(2y-x)] \end{aligned} \quad (11)$$

In the above expression, the constants associated with the sinusoidal functions correspond to the peak current associated with the intermodulation frequency. The non-faradaic current is obtained by substitution of E from equation (8) in equation (5) as shown below.

$$i_{nf} = a_1\omega_1 c_d\cos(x) + a_2\omega_2 c_d\cos(y) \quad (12)$$

Unlike the techniques that employ DC potentials, AV modulation results in non-faradaic currents that do not dissipate even under steady state conditions. As can be seen from the expression (equation 10), the faradic current has several harmonic components, which correspond to (i) multiple (one, two, and three times) of the primary phase shift (i.e. x and y), (ii) the sum as well as the difference in the primary phase shift, and (iii) the sum (as well as the difference) of two times the phase shift of one signal with the phase shift of the other. Thus, the model development paints a picture that describes the faradaic current which is much more complex than what has been described in a previous model that ignores the double-layer capacitance and the solution resistance. Since the experimental data measures the total current, this will correspond to the sum of two currents as given by equations (11) and (12), it would be prudent to carry out experiments at various values of the intermodular frequencies facilitating the estimation of various kinetic parameters as well as the solution resistance and the double-layer capacitance.

The following two simplifying scenarios examine the current response obtained in the absence of a double layer capacitance and the solution resistance.

Case I: $c_d = o$

In the absence of a double-layer capacitance, the non-faradaic current is zero ($i_t = i_f$) according to equation (5). The potential E from equations (1) and (2) can be expressed as:

$$E = E_{DC} + E_{P1}\sin(\omega_1 t) + E_{P2}\sin(\omega_2 t) - i_f R_s \quad (13)$$

Linearization of the Butler Volmer equation as given by (4) yields:

$$i_f \cong \left(\frac{1}{\beta_a} + \frac{1}{\beta_c}\right) i_{corr}(E - E_{corr}) \quad (14)$$

This first approximation allows us to estimate E from equation (13), which is also given by

$$E = a_o + a_1\sin(\omega_1 t) + a_2\sin(\omega_2 t) \quad (15)$$

Where the constants are:

$$a_o = \frac{E_{DC} + R_s i_{corr} E_{Corr}\left(\frac{1}{\beta_a} + \frac{1}{\beta_c}\right)}{1 + R_s i_{corr} E_{Corr}\left(\frac{1}{\beta_a} + \frac{1}{\beta_c}\right)} \quad (15\text{-a})$$

Using the expansion that includes the fourth-order term as given equation (4) and subsequent substitution for the potential as given by equation (15) gives us the following expression for the faradaic current:

$$\begin{aligned} i_f = {} & A + B\sin\omega_1 t + C\sin\omega_2 t + D\cos 2\omega_2 t + E1\cos 2\omega_2 t \\ & + F\sin 3\omega_1 t + G\sin 3\omega_2 t + H[\cos(\omega_1 - \omega_2)t \\ & - \cos(\omega_1 + \omega_2)t] + \frac{I}{2}[\mathrm{Sin}(2\omega_1 + \omega_2)t \\ & - \sin(2\omega_1 - \omega_2)t] + \frac{J}{2}[\mathrm{Sin}(2\omega_2 + \omega_1)t - \sin(2\omega_2 - \omega_1)t] \end{aligned} \quad (16)$$

An important observationi that can be made is that in the absence of the double layer capacitance, the harmonics of the faradaic current will be independent of the shift in the intermodular frequency.

Case II: $R_s = o$

When the solution resistance is zero, due to a lack of the resistance drop: $E_t = E$.

In this case, the solution to the faradaic current will be the same as given by Bosch *et al.*. (1,2). In other words, the shift angle in the harmonics of the intermodular frequency in the observed response will be absent.

The substitution of equation (1) in equation (5) gives us the following expression for the non-faradaic equation:

$$i_{nf} = a_1 \omega_1 c_d \cos \omega_1 t + a_2 \omega_2 c_d \cos \omega_2 t \qquad (17)$$

Thus, the non-faradaic, as well as the total observed current, will not experience any change in the phase.

3. Simulation Parameters

Unless otherwise mentioned in the paper, the following set of data were employed:

$i_{corr} = 7\times10^{-6} A$ cm^{-2}; E_{corr} = -0.33 V; $\beta_a = \beta_c = 0.05$ V;
$C_d = 2\times10^{-6} F$ cm^{-2}; E_{DC} = -0.3 V; $E_{P1} = 0.02$ V;
$E_{P2} = 0.05$ V; $\omega_1 = 2\pi(25)$ *radians/s*;
$\omega_2 = 2\pi(15)$ *radians/s*; and $R_s = 100$ ohms.

4. Results and Discussion

Fig. 2 is a plot of the faradaic current versus time obtained using the expression given by equation (11) as well as the one obtained numerically (equation 6). It is found that the two methods give similar results, except for relatively minor differences observed in the peak currents. The estimated current is observed to be periodic in nature, however, the composite signal in part appears to be non-sinusoidal. The peak of the positive current is 300% greater in magnitude than the corresponding negative peak. Fig. 3 is a plot of the non-faradaic current versus time obtained using equation (12). It is interesting to observe that for the conditions as defined in Figs. 2 and 3, the faradic current is approximately an order of magnitude lower than the non-faradaic current. The data

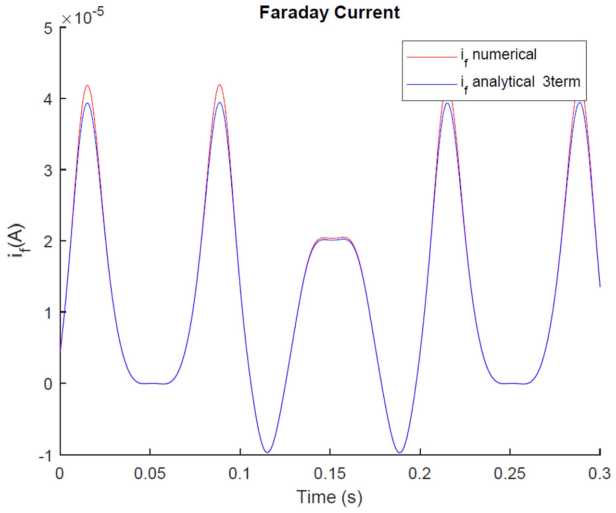

Fig. 2. The faradaic current response of a corroding system in the time domain

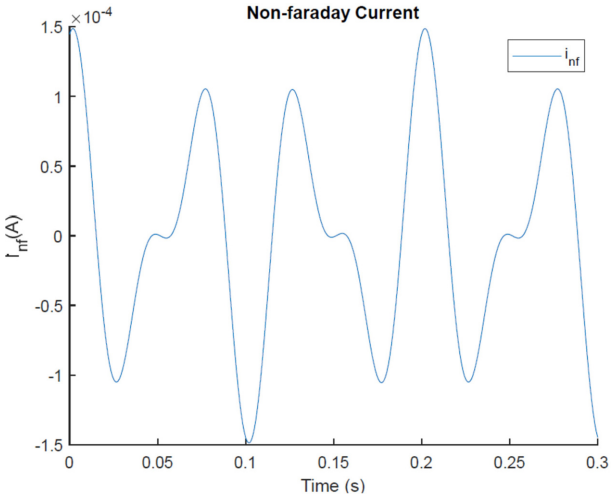

Fig. 3. The non-faradaic current response of a corroding system in the time domain

indicates the significance of the consideration of double-layer capacitance and the electrolyte resistance elements in this study.

One of the important parameters that determines the corrosion characteristics of a given system is the ratio of the anodic to cathodic Tafel slopes $\left(r = \frac{\beta_a}{\beta_c}\right)$. Fig. 4 is a plot of the time average faradaic current vs. the ratio of the anodic to cathodic Tafel slopes for various magnitudes of the corrosion current i_{corr}. It is observed that the faradaic current decreases with the ratio of the two slopes.

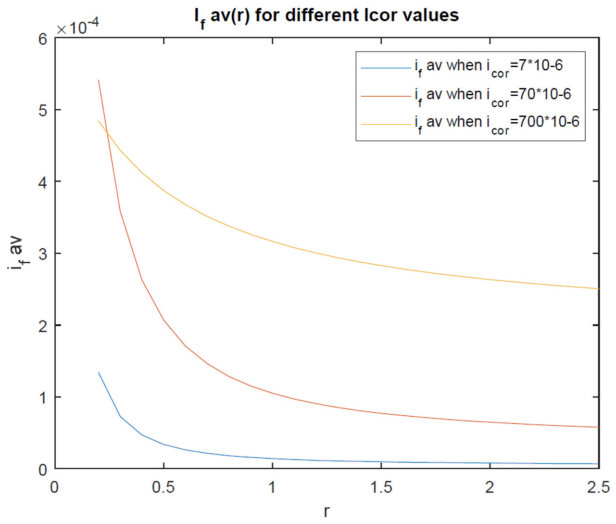

Fig. 4. The average faradaic vs. the anodic-to-cathodic Tafel slope ratio at different corrosion currents

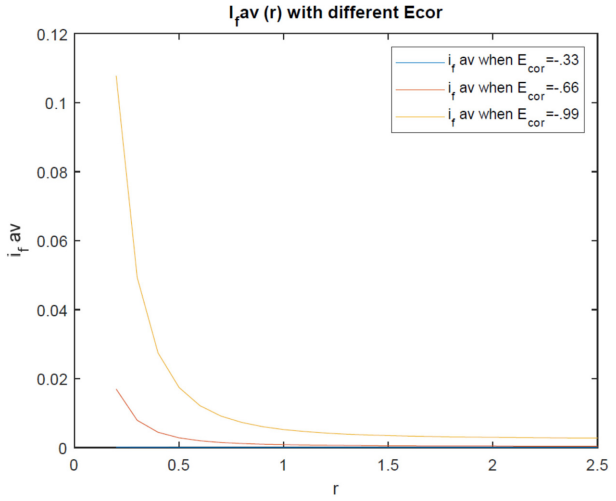

Fig. 5. The average faradaic vs. the anodic-to-cathodic Tafel slope ratio at different corrosion potentials

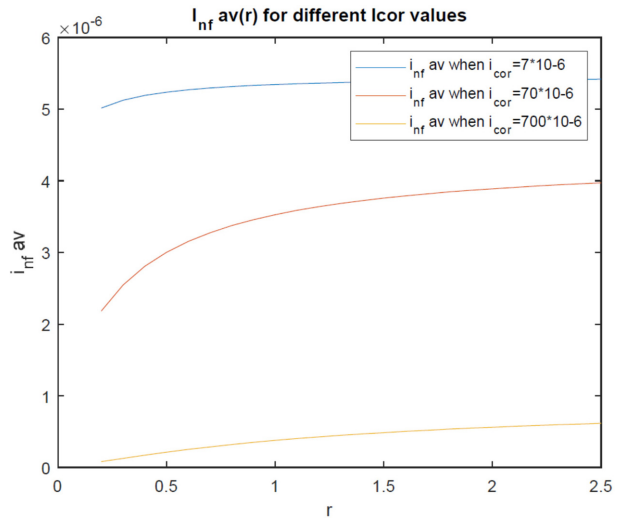

Fig. 6. The non-faradaic vs. the anodic-cathodic Tafel slope ratio at different corrosion currents

According to equation (9), the faradaic current is proportional (non-linearly) to the potential across the double layer as well as the following coefficients: α_1, β_1, and γ_3 which are functions of r as shown in Appendix. At a relatively high ratio of the anodic to cathodic Tafel slope (r), the β_1 and γ_3 terms decrease in magnitude, while α_1 increases linearly, thus according to equation (9) the relationship between the faradaic current and the anodic to cathodic Tafel slope ratio seems to be linear. The opposite is true in the case of relatively low values of the Tafel slope ratio, r. Thus, the analysis shows that especially for the relatively low values of the Tafel slope ratio, the influence of the higher-order terms of the potential, E (equation 9) is significant, and thus they may not be ignored in the analysis. Another observation that can be made by examining Fig. 4 is that higher corrosion rate results in greater faradaic (average) current especially when the ratio of the anodic-to-cathodic Tafel slope is relatively high (i.e., greater than 0.5) in accordance with equation (9).

Fig. 5 shows that the average faradaic current decreases with the anodic-to-cathodic Tafel slope ratio for a given corrosion potential especially at relatively small values of r. However, when the corrosion potential is nobler (0-0.33 V vs SCE), the faradaic current is almost negligible and independent of r. As the corrosion potential becomes more active, the correspondingly higher average faradaic current is observed. Concerning the average non-faradaic current, simulations show that it increases with the anodic-to-cathodic Tafel slope ratio, and that an increase in the corrosion current results in a correspondingly lower non-faradaic current (Fig. 6). A comparison of the average faradaic current and the average non-faradaic current (Figs. 4 and 6) shows that the former is greater than the latter, thus averaging of the current has an effect of lowering the average non-faradaic current as explained below. This appears to be in contrast with the data on two currents as a function of time (Figs. 2 and 3). An examination of the expressions derived for the faradaic as well as the non-faradaic currents (equations 11 and 11)

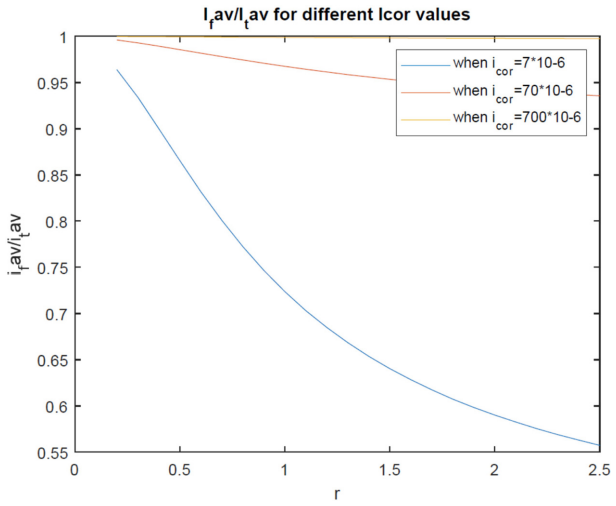

Fig. 7. The ratio of the average of the faradic to the average of the non-faradaic current vs. the anodic-cathodic Tafel slope ratio at different corrosion currents

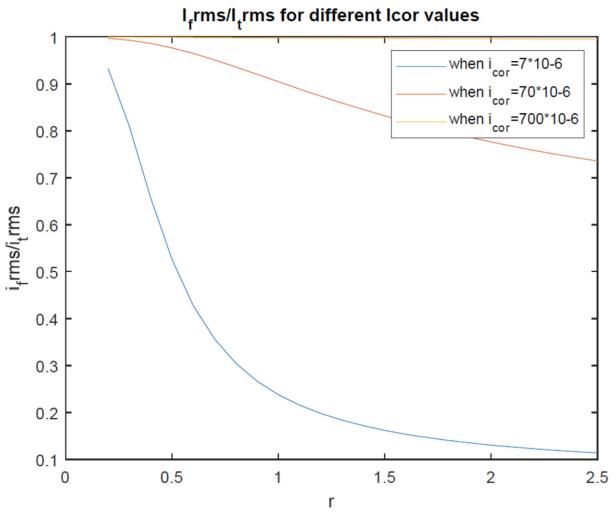

Fig. 8. The ratio of the average of the faradic to the average of the non-faradaic current vs. the anodic-cathodic Tafel slope ratio at different corrosion currents

shows that averaging (i.e. integration of the current vs time function), has a much greater influence in reducing the non-faradaic current than it has a corresponding effect on lowering the faradaic currents because the latter has several components corresponding to the multiples of the input signal frequencies (i.e. $2\omega_2$, $2\omega_1$, $3\omega_2$, $3\omega_1$) and other complex forms of the input signal frequencies ($\omega_2 - \omega_1$, $\omega_2 + \omega_1$), which do not yield non-zero numbers., while the latter (i.e. non-faradaic current) has the components that correspond to the primary input frequencies (ω_2, ω_1).

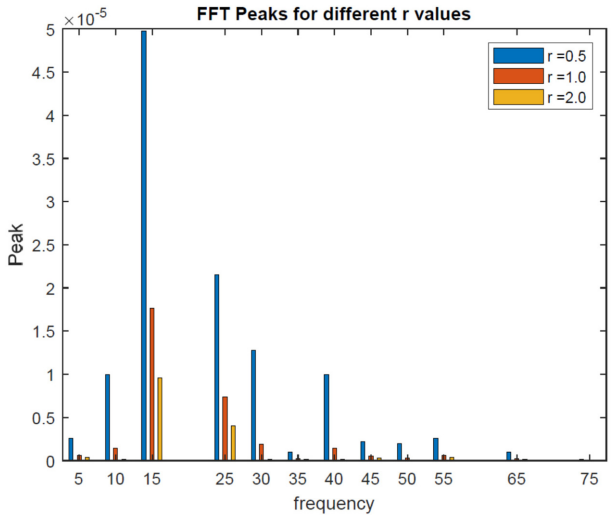

Fig. 9. The peak current (A) response of a corroding system vs. the frequency (Hz) domain at different anodic-to-cathodic Tafel slope ratio

Thus, a comparison of the average faradaic and non-faradaic currents must be made very carefully. Fig. 7 is a plot of the ratio of the averages of the total faradaic current to the total (sum of faradaic and non-faradaic) current as a function of the Tafel slope ratio at three different corrosion current values. The data show that for the low anodic-to-cathodic Tafel slope ratio, the current ratio is one, however, it decreases at high anodic Tafel slope values. Also, the deviation of the total current (average) from the faradaic current (average) increases substantially with the corrosion current. Thus, if a material is known to have a high corrosion current, the measured current (i.e., the total current) will be considerably higher than the faradaic current. The root-mean-square current, the total current as well as the faradaic current were also computed. The ratio of the RMS faradaic to the total RMS current vs the anodic-to-cathodic Tafel slope ratio for three different corrosion currents is shown in Fig. 8. The data show that $i_{f,\,rms}$ increases with the anodic-to-cathodic Tafel slope ratio while it decreases with the corrosion current. This analysis is of the consequence when power analysis of the corrosion system is performed.

Another important feature of the EFM is that it can be analyzed using FFT, which in turn allows for the determination of the corrosion characteristics. The Fast Fourier Transform function available in M (Matlab) was employed to find the peak harmonics corresponding to the faraday current signal. A sampling frequency of 200

Table 1. Peak current relative to the peak value for 15 Hz (ω_2)signal as a function of the ratio of the anodic-to-cathodic Tafel slope (r) Quantity in the parenthesis represents the peak current (*10^3) for 15 Hz signal

Frequency, Hz (angular frequency, rad/s)	r = 0.2	r = 0.5	r = 0.8	r = 1.0	r = 1.5	r = 2.0
15 (ω_2)	1.00 (0.3534)	1.00 (0.0498)	1.00 (0.0235)	1.00 (0.0177)	1.00 (0.0118)	1.00 (0.0096)
25 (ω_1)	0.47	0.43	0.42	0.42	0.42	0.42
30 ($2\omega_2$)	0.38	0.26	0.15	0.11	0.03	0.01
40 ($\omega_1 + \omega_2$)	0.30	0.20	0.12	0.08	0.03	0.01
10 ($\omega_1 - \omega_2$)	0.30	0.20	0.12	0.08	0.03	0.01
5 ($2\omega_2 - \omega_1$)	0.09	0.05	0.04	0.03	0.03	0.03
55 ($2\omega_2 + \omega_2$)	0.09	0.05	0.04	0.03	0.03	0.03
45 ($3\omega_2$)	0.08	0.04	0.03	0.03	0.03	0.03
50 ($2\omega_1$)	0.06	0.04	0.02	0.02	0.00	0.00
65 ($2\omega_1 + \omega_2$)	0.04	0.02	0.01	0.01	0.02	0.01
35 ($2\omega_1 - \omega_2$)	0.04	0.02	0.01	0.01	0.02	0.01

Hz was used while the length of the signal was considered to be 2000. A simulation involving five different values of the ratio of the anodic-to-cathodic Tafel slopes was performed. The results (Table 1) show that the most prominent peak obtained corresponds to the input signal with the highest amplitude (ω_2 of 15 cycles/second) while the next prominent peak corresponds to the input signal with a lower amplitude (ω_1 of 25 cycles/second). The harmonics obtained were found to correspond to the various sums of the two principal frequencies as shown in the table. Two observations are made: (i) in general the peak currents decreases with the ratio of the anodic-to-cathodic Tafel slope, and (ii) the harmonics corresponding to various multiples of the input signal frequencies decrease in significance in the following manner:

$$i_{p,\,\omega_2} > i_{p,\,\omega_1} > i_{p,\,2\omega_2} > i_{p,\,\omega_2+\omega_1} = i_{p,\,-\omega_2+\omega_1} > i_{p,\,2\omega_2+\omega_1} = i_{p,\,2\omega_2+\omega_1} > i_{p,\,3\omega_2} > i_{p,\,2\omega_1} > i_{p,\,\omega_2+2\omega_1} = i_{p,\,-\omega_2+2\omega_1}$$

Where i_p corresponds to the peak harmonic corresponding to the particular frequency as specified by the subscript in the notation. The various peak currents correspond to

Table 2. The shift in the phase to primary frequency vs. the anodic-to-cathodic Tafel slope ratio (r)

Anodic-to-Cathodic Tafel Slope Ratio (r)	ϕ_1	ϕ_2
0.2	1.32	1.42
0.5	1.26	1.38
0.8	1.21	1.35
1	1.17	1.32
1.5	1.08	1.26
2	1.00	1.21

the constants associated with the sinusoidal functions listed in equations (10), for example, B = i_{p,ω_1}, C= $i_{p,2\omega_2}$ and so on. The shift (ϕ) in the phase angle calculated using equation (A-7) is found to be of order one for all values of the anodic-to-cathodic Tafel slope ratios examined in this study. The shift in the phase angle is found to decrease slightly with the slope ratio and it reaches unity for the anodic-to-cathodic Tafel slope of 2.

5. A Comparative Study

A comparison of the present model with the predictions made by the previous model using the data used for simulation of Obot *el al.* [8] is shown in Fig. 10. The data clearly show that by factoring in the solution resistance and double layer capacitance, the total current observed is as high as 2.5 times predicted by the original EFM model [1,2]. In addition, the non-faradaic current is also found to be of significance in relation to the fardaic current. The data are obtained for the case when the applied voltage signals are assumed to be 2 and 5 Hz.

Even a more dramatic rise in the differences between currents corresponding to the model proposed here and the original model are observed when the applied potential signals imposed have higher frequencies (15 and 25 Hz). The ratio of the actual peak current (this model) to the current predicted by the previous model is observed to be approximately 6.3. This is in line with the fact that the double layer capacitance current increases linearly with the signal frequency.

6. Conclusions

As compared to the previous EFM model, the analysis presented here not only accounts for the presence of the solution resistance and the double layer capacitance, it also explores the application of intermodular frequency signals whose peak magnitudes are not equal to one another. In addition, it allows for the application of a non-zero DC signal.

The data show that the potential across the impedance which is responsible for the generation of the faradaic current involves a shift in the phase angle of the imposed sinusoidal signals, a finding which is at variance from the earlier studies. As a result, the current generated is a function of the phase angle shift.

For two special cases that involve the absence of

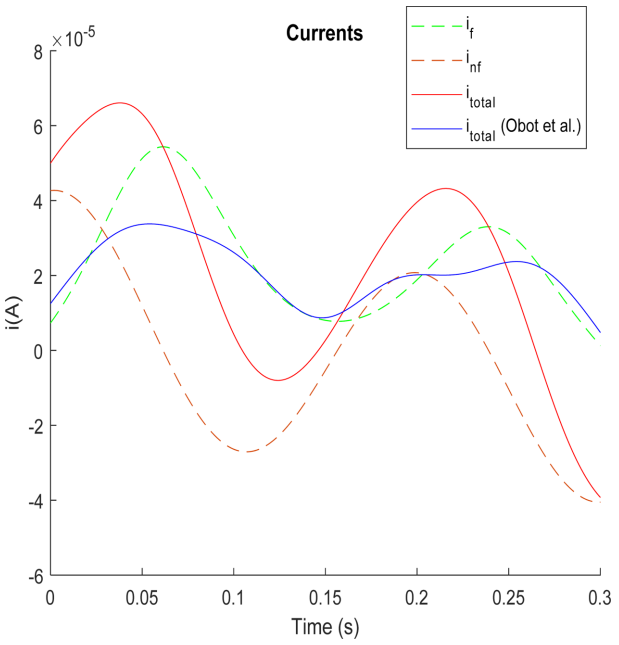

Fig. 10. The peak current (A) response of a corroding system vs. time The peak potentials and frequencies of the applied signals correspond to 50 mV, and 2 and 5 Hz respectively

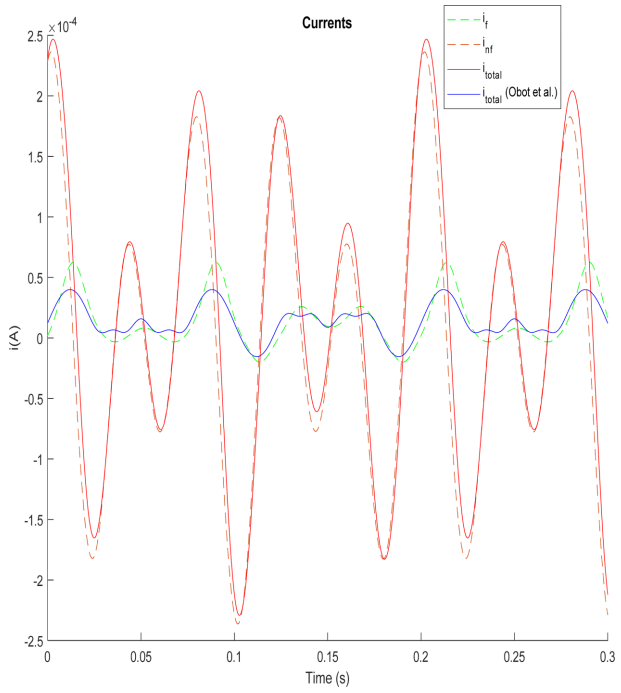

Fig. 11. The peak current (A) response of a corroding system vs. time The peak potentials and frequencies of the applied signals correspond to 50 mV, and 15 and 25 Hz respectively

solution resistance and the double layer capacitance, the resulting current will not experience a shift in the phase angle with respect to the imposed intermodular frequency signal.

Appendix

$$\alpha = \frac{i_{corr}\alpha_1}{c_d} + \frac{1}{R_s c_d} \quad \text{(A-1)}$$

$$\alpha_1 = \left(\frac{1}{\beta_a} + \frac{1}{\beta_c}\right) = \frac{1}{\beta_a}(1 + r) \quad \text{(A-2)}$$

$$\text{Where } r = \frac{\beta_a}{\beta_b} \quad \text{(A-2-1)}$$

$$\beta_1 = \frac{1}{2}\left(\frac{1}{\beta_a^2} - \frac{1}{\beta_c^2}\right) = \frac{1}{2\beta_a^2}(1 - r^2) \quad \text{(A-3)}$$

$$\gamma_1 = \frac{E_{P1}}{R_s c_d} \quad \text{(A-4)}$$

$$\gamma_2 = \frac{E_{P2}}{R_s c_d} \quad \text{(A-5)}$$

$$\gamma_3 = \frac{1}{6}\left(\frac{1}{\beta_a^3} - \frac{1}{\beta_c^3}\right) = \frac{1}{6\beta_a^2}(1 - r^3) \quad \text{(A-6)}$$

$$\varphi_1 = \tan^{-1}\left(\frac{\omega_1}{\alpha}\right) \quad \text{(A-7)}$$

$$\varphi_2 = \tan^{-1}\left(\frac{\omega_2}{\alpha}\right) \quad \text{(A-8)}$$

$$\lambda = \frac{E_{DC}}{R_s c_d} + \left(\frac{i_{corr}\alpha_1}{c_d}\right)E_{corr} \quad \text{(A-9)}$$

$$a_o = \frac{\lambda}{\alpha} \quad \text{(A-10)}$$

$$a_1 = \frac{\gamma_1 \cos(\phi_1)}{\alpha} \quad \text{(A-11)}$$

$$a_2 = \frac{\gamma_2 \cos(\phi_2)}{\alpha} \quad \text{(A-12)}$$

$$A = [\alpha_1 a_o + \beta_1\left(a_o^2 + \frac{1}{2}a_1^2 + \frac{1}{2}a_2^2\right) + \gamma_3\left(a_o^3 + \frac{3}{2}a_o a_1^2 + \frac{3}{2}a_o a_2^2\right)]i_{corr} \quad \text{(A-13)}$$

$$B = \left[\alpha_1 a_1 + 2\beta_1 a_o a_1 + 3\gamma_3(a_o^2 a_1 + \frac{a_1^3}{4} + \frac{a_1 a_2^2}{2})\right]i_{corr} \quad \text{(A-14)}$$

$$C = \left[\alpha_1 a_2 + 2\beta_1 a_o a_2 + 3\gamma_3(a_o^2 a_2 + \frac{a_2^3}{4} + \frac{a_2 a_1^2}{2})\right]i_{corr} \quad \text{(A-15)}$$

$$D = -\frac{a_1^2}{2}(\beta_1 + 3a_o\gamma_3)i_{corr} \quad \text{(A-16)}$$

$$E1 = -\frac{a_2^2}{2}(\beta_1 + 3a_o\gamma_3)i_{corr} \quad \text{(A-17)}$$

$$F = -\frac{a_1^3}{4}\gamma_3 i_{corr} \quad \text{(A-18)}$$

$$G = -\frac{a_2^3}{4}\gamma_3 i_{corr} \quad \text{(A-19)}$$

$$H = a_1 a_2(\beta_1 + 3a_o\gamma_3)i_{corr} \quad \text{(A-20)}$$

$$I = -\frac{3}{2}a_1^2 a_2 \gamma_3 i_{corr} \quad \text{(A-21)}$$

$$J = -\frac{3}{2}a_1 a_2^2 \gamma_3 i_{corr} \quad \text{(A-22)}$$

References

1. R. W. Bosch, J. Hubrecht, and W. F. Bogarets, On-line corrosion monitoring using electrochemical frequency modulation (EFM), EPRI, Final Report, TR-112786, April (1999).
2. R.W. Bosch, J. Hubrecht, and W. F. Bogaerts, and B. C. Syrett, Electrochemical Frequency Modulation: a New Electrochemical Technique for Online Corrosion Monitoring, *Corrosion*, **57**, 60 (2001). Doi: https://doi.org/10.5006/1.3290331
3. G. P. Rao and A. K. Mishra, A.C. techniques to evaluate the kinetics of corrosion kinetics, *Journal of Electroanalytical Chemistry and Interfacial Electrochemistry*, **77**, 121 (1977). Doi: https://doi.org/10.1016/S0022-0728(77)80326-4
4. U. Bertocci, AC induced corrosion. The effect of an alternating voltage on electrodes under charge-transfer control, *Corrosion*, **35**, 211 (1979) . Doi: https://doi.org/10.5006/0010-9312-35.5.211
5. L. Mészáros and J. Dévay, Study of the rate of corrosion of metals by a faradaic distortion method III. – Determination of the kinetic parameters of the corrosion process by intermodulation distortion, *Acta Chimica Academiae Scientarium Hungaricae*, **105**, 1 (1980). Doi: http://www.khde-sign.co.uk/acrobat/meszaros3.pdf
6. S. S. Abdel-Rehim, K. F. Khaled, and N. S. Abd-Elshafi, Electrochemical frequency modulation sa a new tech-

nique for monitoring corrosion behavior of iron in acid media by new thiourea derivative, *Electrochemica Acta*, **51**, 3269 (2006). Doi: https://doi.org/10.1016/j.electacta.2005.09.018

7. A. Rauf and E. Mahdi, Comparison between electrochemical noise and electrochemical frequency modulation measurements during pitting corrosion, *Journal of New Materials for Electrochemical Systems*, **15**, 107 (2012). Doi: https://doi.org/10.14447/jnmes.v15i2.79
8. I. B. Obot and I. B. Onyeachu, Electrochemical frequency modulation (EFM) technique: Theory and recent practical applications in corrosion research, *Journal of Molecular Liquids*, **249**, 83 (2018). Doi: https://doi.org/10.1016/j.molliq.2017.11.006
9. A. Singh, K. F. Ansari, E. Ituen, L. Guo, M. A. Wahab, M. A. Quraishi, X. Kong, and Y. Lin, A new series of synthesized compounds as corrosion mitigator for storage tanks: detailed electrochemical and theoretical investigations, *Construction and Building Materials*, **259**, October, No. 120421 (2020). Doi: https://doi.org/10.1016/j.conbuildmat.2020.120421
10. I. Danaee and P. Nikpiarsa, Application of quantum chemical, noise and electrochemical frequency modulation to investigate the adsorption and corrosion inhibition bevaior of 2-amino-6-hydroxybenothiazole for steel API X80 in acidic solution, *Journal of the Chilean Chemical Society*, **65**, 4708 (2020). Doi: https://www.jcchems.com/index.php/JCCHEMS/article/view/1017
11. A. Rauf and W. F. Bogaerts, Employing electrochemical frequency modulation for pitting corrosion, *Corrosion Science*, **52**, 2773 (2010). Doi: https://doi.org/10.1016/j.corsci.2010.04.016
12. A. Rauf, W. F. Bogaerts, and E. Mahdi, Implementation of Electrochemical Frequency Modulation to Analyze Stress Corrosion Cracking, *Corrosion*, **68**, #035002-1 - 035002-8 (2012). Doi: https://doi.org/10.5006/1.3691836
13. A. Rauf and E. Mahdi, Evaluating Corrosion Inhibitors with the help of electrochemical measurements including electrochemical frequency modulation, *International Journal of Electrochemical Science*, **7**, 4673 (2012). Doi: http://www.electrochemsci.org/papers/vol7/7054673.pdf
14. S. Lalvani, L. Kerr, S. Lalvani, D. Olaguera-Delogu, A Critical Review of Electrochemical Frequency Modulation: Revision of Previous Model, submitted to *Journal of the Electrochemical Society.*
15. R. Zhang, P. R. Vairavanathan, and S. B. Lalvani, Perturbation Method Analysis of AC-induced Corrosion, *Corrosion Science*, **50**, 1664 (2008). Doi: https://doi.org/10.1016/j.corsci.2008.02.018